TRANSONIC UNSTEADY SEPARATED FLOW OVER PROFILE

Vladislav Pafnutiev
Moscow Institute of Physics and Technology,
16 Gagarin St., Zhukovsky, Moscow Region, 140160 RUSSIA

Keywords: *Navier-Stockes equations, transonic flow, unsteady flow, profile*

Abstract

Transonic unsteady separated flow over profile at different angle of attract is considered. Airflow simulation was made by numerical solution of the Navier-Stockes equations for laminar and turbulent flow models. Two-equations differential turbulence model were used in the last case. Unsteady flow results for some cases were obtained and investigated.

1 Introduction

Last time the great interest is being paid to an investigation of airfoils in the transonic airflow [1]. Overcoming of sonic barrier by aircrafts is extremely actual for increasing of all types aviation's efficiency.

The greatest part of investigations (i.e. [1,4]) on airfoils in transonic flows considers cases when free stream Mach number is subsonic (M_∞=0.6-0.8). The cases are due to actual flight velocities of modern civil airplanes. Nevertheless the cases of free stream Mach number M_∞=0.9-1.2 were investigated rarely. But this range of Mach numbers is the most interesting and complicated from the aerodynamics point of view. At these velocities aerodynamic features such as supersonic zones, shockwave – boundary layer interactions, shockwave – separated flow interactions occur.

Difficulties in modeling of transonic airflow (M_∞=0.9-1.2) in ground tests are due to hard flow perturbations induced by shockwave reflection on perforated wind-tunnel walls [3]. Thus methods based on numerical solution of the Navier-Stockes equations are used for modeling of these types of airflows.

In this paper the problem of NACA-0012 and double-edge profiles in transonic flow for laminar and turbulent airflow models is being investigated. The most attention is paid to behavior of aerodynamic coefficients and to flow field over airfoil at the angle of attack at overcoming of the sonic barrier.

2 Numerical simulation

Reynolds-averaged Navier-Stokes equations utilizing mass-weighted averaging in arbitrary curvilinear coordinate system (ξ,η) can be expressed in conservation form as

$$\frac{\partial \mathbf{Q}}{\partial t}+\frac{\partial \mathbf{E}}{\partial \xi}+\frac{\partial \mathbf{G}}{\partial \eta}=\mathbf{B}$$

Q, **E**, **F**, and **B** vectors are connected with correspondent $\mathbf{Q}_c$, $\mathbf{E}_c$, $\mathbf{G}_c$ and $\mathbf{B}_c$ vectors in the Cartesian system by expressions

$$\mathbf{Q}=J\mathbf{Q}_c, \quad \mathbf{E}=J\left(\mathbf{E}_c\frac{\partial \xi}{\partial x}+\mathbf{G}_c\frac{\partial \xi}{\partial y}\right),$$

$$B=JB_c, \quad \mathbf{G}=J\left(\mathbf{E}_c\frac{\partial \eta}{\partial x}+\mathbf{G}_c\frac{\partial \eta}{\partial y}\right),$$

$J=\partial(x,y)/\partial(\xi,\eta)$, $x=x(\xi,\eta)$, $y=y(\xi,\eta)$. Cartesian components of $\mathbf{Q}_c$, $\mathbf{E}_c$, $\mathbf{G}_c$ and $\mathbf{B}_c$ for 2-D Reynolds-averaged Navier-Stokes equations (with using of Favre-averaging) have the forms

$$\mathbf{Q}_c = \left\| \begin{matrix} \rho \\ \rho u \\ \rho v \\ \rho(e+q^2) \\ \rho q \\ \rho \omega \end{matrix} \right\|, \quad \mathbf{E}_c = \left\| \begin{matrix} \rho u \\ \rho u^2 + p + \frac{2}{3}\rho q^2 + \tau_{xx} \\ \rho uv + \tau_{xy} \\ \rho uH + \frac{5}{3}\rho u q^2 + I_x \\ \rho uq + I_x^q \\ \rho u\omega + I_x^\omega \end{matrix} \right\|,$$

$$\mathbf{G}_c = \left\| \begin{matrix} \rho v \\ \rho uv + \tau_{xy} \\ \rho v^2 + p + \frac{2}{3}\rho q^2 + \tau_{yy} \\ \rho vH + \frac{5}{3}\rho v q^2 + I_y \\ \rho vq + I_y^q \\ \rho v\omega + I_y^\omega \end{matrix} \right\|, \quad \mathbf{B}_c = \left\| \begin{matrix} 0 \\ 0 \\ 0 \\ 0 \\ h_1\rho\omega q \\ h_2\rho\omega^2 \end{matrix} \right\|,$$

where

$e=h-p/\rho+(u^2+v^2)/2, \quad H=h+(u^2+v^2)/2, \quad h=CpT$

stress tensor $\boldsymbol{\tau}$ has the components

$$\tau_{xx} = (\mu+\mu_T)(\frac{2}{3}\mathrm{div}\mathbf{V} - 2\frac{\partial u}{\partial x}),$$

$$\tau_{xy} = -(\mu+\mu_T)(\frac{\partial u}{\partial y}+\frac{\partial v}{\partial y}),$$

$$\tau_{yy} = (\mu+\mu_T)(\frac{2}{3}\mathrm{div}\mathbf{V} - 2\frac{\partial y}{\partial y}),$$

heat flux vector $\mathbf{I}$, $\mathbf{I}^q$,$\mathbf{I}^\omega$ is determined as

$$\mathbf{I} = -(\lambda+\lambda_T)\mathrm{grad}(T) + \boldsymbol{\tau}\mathbf{V}$$

$$\mathbf{I}^q = -(\mu + \frac{\mu_T}{\mathrm{Pr}_1})\mathrm{grad}(q)$$

$$\mathbf{I}^\omega = -(\mu + \frac{\mu_T}{\mathrm{Pr}_2})\mathrm{grad}(\omega)$$

To close the mass-averaged Navier-Stokes equations Coakley and Huang [5] two equations differential turbulent model q - ω was used

$$q = \sqrt{k}, \quad \omega = \varepsilon/k,$$

$$\mu_T = C_\mu f\rho q l = C_\mu f \frac{\rho q^2}{\omega}, C_\mu = 0.09,$$

$$f = 1 - \exp(-\alpha\frac{\rho r_w q}{\mu}), \alpha = 0.02,$$

$$h_1 = C_{11}(C_\mu f \frac{S}{\omega^2} - \frac{2}{3}\frac{\mathrm{div}\mathbf{V}}{\omega}) - C_{12},$$

$$h_2 = C_{21}(C_\mu \frac{S}{\omega^2} - C_{23}\frac{\mathrm{div}\mathbf{V}}{\omega}) - C_{22},$$

$$S = \frac{4}{3}[\left(\frac{\partial u}{\partial x}\right)^2 - \frac{\partial u}{\partial x}\frac{\partial v}{\partial y} + \left(\frac{\partial v}{\partial y}\right)^2] + (\frac{\partial u}{\partial y}+\frac{\partial v}{\partial x})^2$$

$$\mathrm{div}\mathbf{V} = \frac{\partial u}{\partial x} + \frac{\partial v}{\partial y}$$

where y is the distance from the wall,

$C_{11}=C_{12}=1, C_{22}=0.833, C_{23}=2.4,$
$C_{21}= 0.055 + 0.5\, f(q,r_w,\rho,\mu), \; Pr_1=Pr_2=2$

Perfect gas state equation $p=\rho RT/M$, where R is the universal gas constant, M is a molar mass; the dependence of molecular viscosity coefficient upon the temperature by the expression

$$\mu/\mu_\infty = \frac{(T/T_\infty)^{1.5}\times(1+110.4/T_\infty)}{T/T_\infty + 110.4/T_\infty},$$

and the constant condition of the Prandtl numbers $Pr=\mu c_p/\lambda=0.7$, $Pr_T=\mu_T c_p/\lambda_T=0.9$ were given.

The no-slip conditions, adiabatic boundary condition $\partial T_w/\partial n=0$, $q_w=0$, $\partial\omega_w/\partial n=0$ were given on the solid wall boundary (η=0).

Reflection boundary conditions written in Riemann invariants were given on the outer boundary (η=0).

The grid line corresponding to ξ=0 was coincide with line corresponding to ξ=1 and periodic conditions $\mathbf{Q_c}\,|_{(\xi=1)} = \mathbf{Q_c}\,|_{(\xi=0)}$ were used.

Development of numerical grid was based on the differential methods. Three zones of

$1/Re$, $2/Re^{1/2}$, $1.5/Re^{1/5}$ thickness were chosen in the vicinity of solid wall. There were 6%, 20% and 25% of total nodes number along the normal coordinate within each of these zones, respectively.

Numerical algorithm is based on the monotone finite-volume difference TVD scheme with the approximation solution of Riemann problem and Newton method to solve differences equations. To approximate the viscous part of the flux vector the second order central differences-type scheme was used. The generation of Jacobi matrix was made by finite differences approach. To accelerate the convergence of iteration process the generation of Jacobi matrix was made on the truncated stencil of 3×3 sizes including mixed derivatives. A solution of linear algebraic system on each nonlinear iteration was made by variational iteration method. This method consists of an incomplete LU-decomposition and a generalized minimal residual algorithm (GMRES). The method of incomplete decomposition by position has been used, because of this technique is extremely simple to implement, does not require much memory or involve a large number of operations, and operates quite satisfactorily in most cases. More detailed the numerical approach used was described in Ref. [6].

3 Results of investigation

All numerical results were obtained with the using of 301×101 grid. The average time needed to calculate one variant was about 10 CPU hours of Pentium-III PC with the optimization of calculations by modified Newton-Raphson method with re-calculation of Jacobi matrix on truncated stencil 3×3.

Numerical investigations were provided for transonic turbulent overflow profile NACA-012 and double-edge profile. The free stream conditions were: Mach number M_∞=0.9, 1.0, 1.2, 1.5, angle of attack α: 0^0-30^0 with 5^0 step, Reynolds number $Re=10^6$, dimensionless turbulence parameters q_∞=0.03, w_∞=40.0. Unsteady investigations were provided for laminar airflow double-edge and NACA profiles, M_∞=0.9, $Re_\infty = 10^6$.

Selected Reynolds number is corresponded to the case of laminar-turbulent transition on the profile surface or in profile vicinity.

In turbulent case of flow steady state solutions were obtained for all freestream conditions. In laminar flow the solution was unsteady for Mach number M_∞=0.9 while for Mach number greater then M_∞=0.9 airflow was steady too. Coefficients represented below are corresponded to steady case. For unsteady case (M_∞=0.9) the coefficients are time averaging.

Drag, lift, pitching coefficients and aerodynamic center position is given by the equations:

$$c_x = c_{xf} + c_{xp},\ c_{xp} = \oint c_p dy,\ c_{xf} = \oint c_f dx,$$

$$c_y = c_{yf} + c_{yp},\ c_{yf} = \oint c_f dy,\ c_{yp} = \oint c_p dx,$$

$$m_z = \oint ((c_{yf} + c_{yp}) \cdot \bar{x} - (c_{xf} + c_{xp}) \cdot \bar{y}) d\bar{l}$$

$$\bar{x} = x/L, \bar{y} = y/L,$$

$$X_f = m_z / c_y,$$

$$c_p = \frac{p - p_\infty}{0.5 \times \rho_\infty \times V_\infty^2 \times L},\ c_f = \frac{\mu \dfrac{\partial V}{\partial n}}{0.5 \times \rho_\infty \times V_\infty^2 \times L},$$

Were L is length of profile chord and V is full velocity.

3.1 Profile transonic airflow results

Dependences of main aerodynamic coefficients on angle of attack ($0° \le \alpha \le 15°$) for NACA-0012 airfoil are represented in Figs. 1-4. Drag coefficient for turbulent model is less then one for laminar case in subsonic flow M_∞=0.9 (Fig. 1). While for M_∞=1 reversed situation occurs. Nevertheless the point corresponding to M_∞=1 and α=15° is not under the regularity (Fig. 1-3). This situation arises due to separation point displacement toward to leading edge and due to the generation of global separated flow.

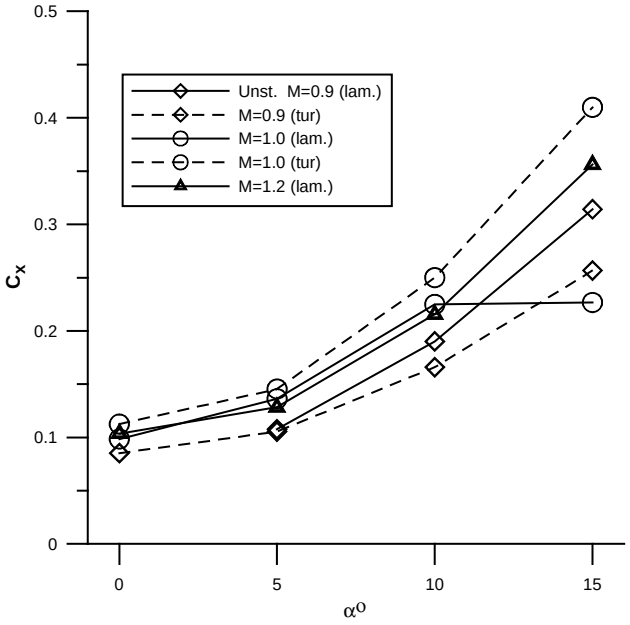

Fig. 1. Dependence of drag coefficient on angle of attack α for different Mach numbers.

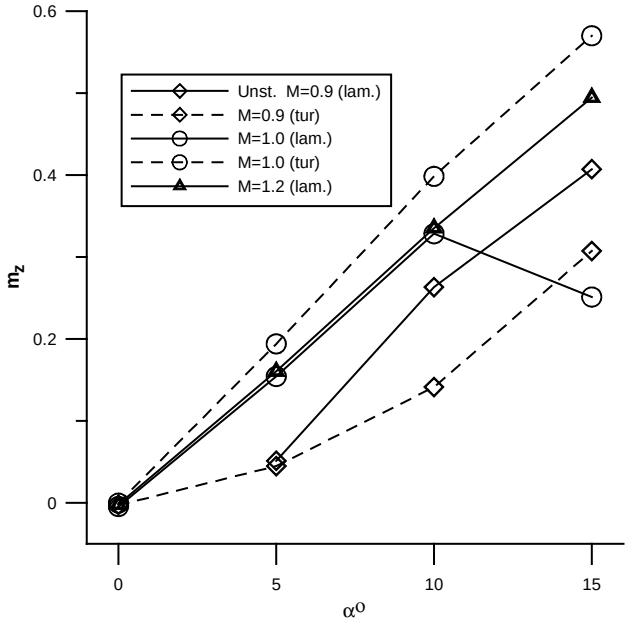

Fig. 3. Dependence of pitching coefficient on angle of attack α for different Mach numbers

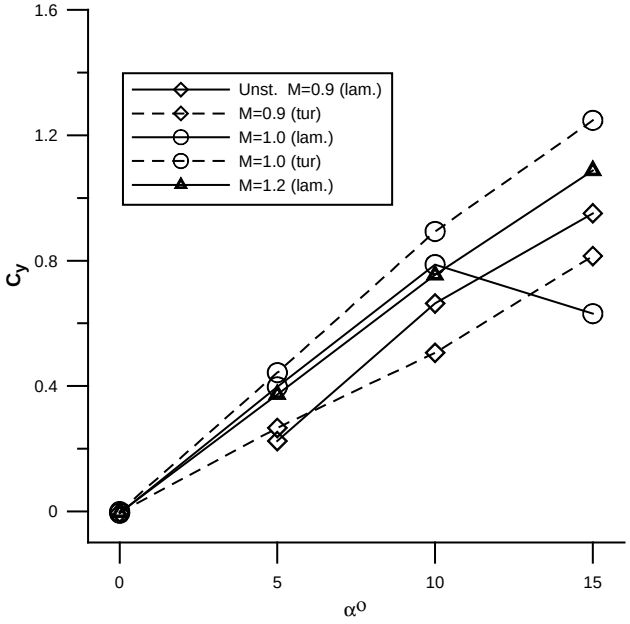

Fig. 2. Dependence of lift coefficient on angle of attack α for different Mach numbers.

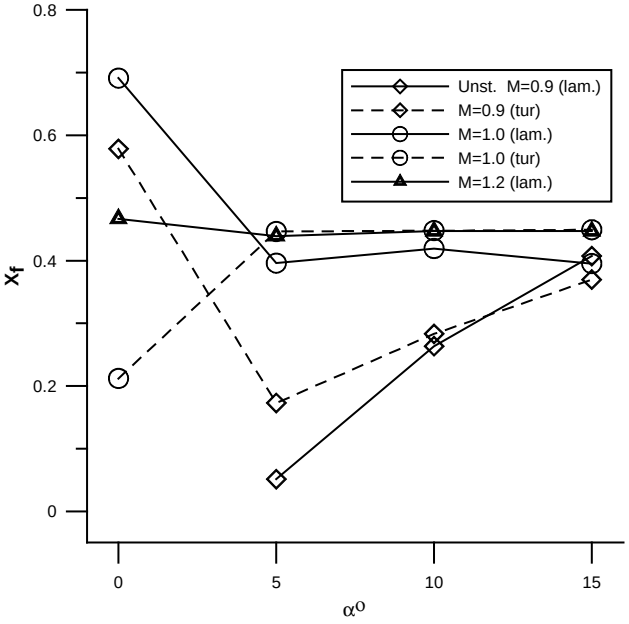

Fig. 4. Dependence of focus position on angle of attack α for different Mach numbers.

Dependence of lift coefficient on freestream Mach number (Fig. 5) shows that the maximum of lift corresponded to Mach number M_∞=1. In this case the mechanism of lift generation is changed.

The change in aerodynamic center position at the overcoming of sonic barrier (Fig.6) illustrates well-known regularity: the aerodynamic center position is situated at 1/4 chord length for subsonic flows, for supersonic flows it is displaced to the 1/2 chord length.

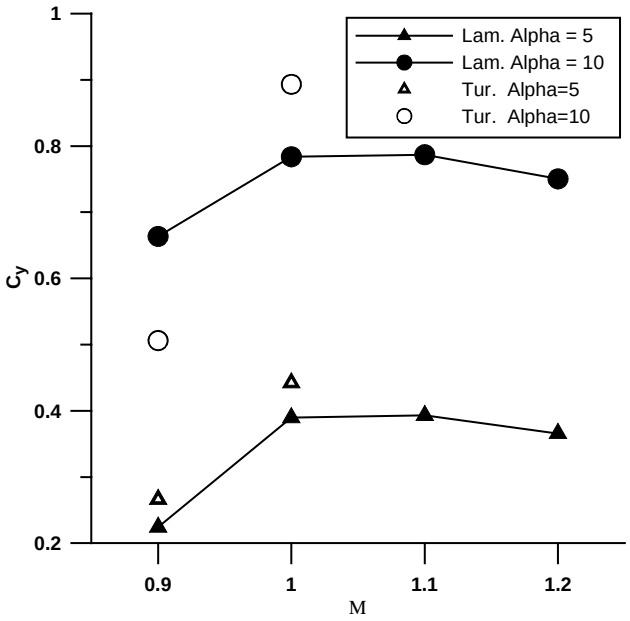

Fig. 5. Dependence of lift coefficient on Mach number M for laminar and turbulent cases.

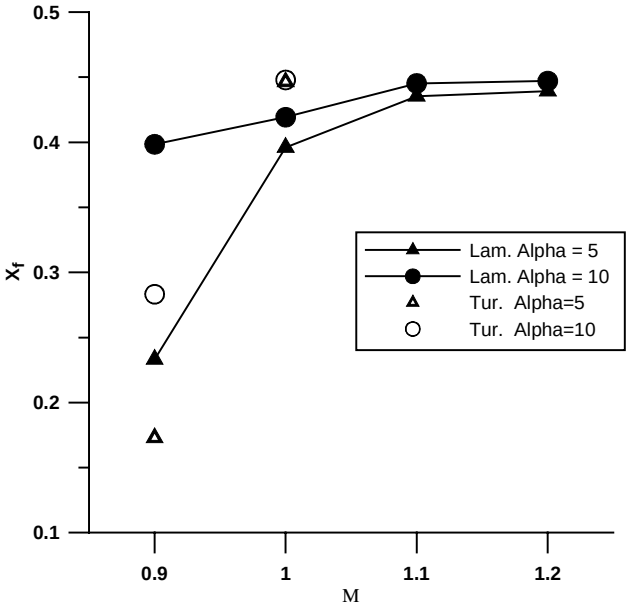

Fig. 6. Dependence of aerodynamic center position on Mach number M for laminar and turbulent cases.

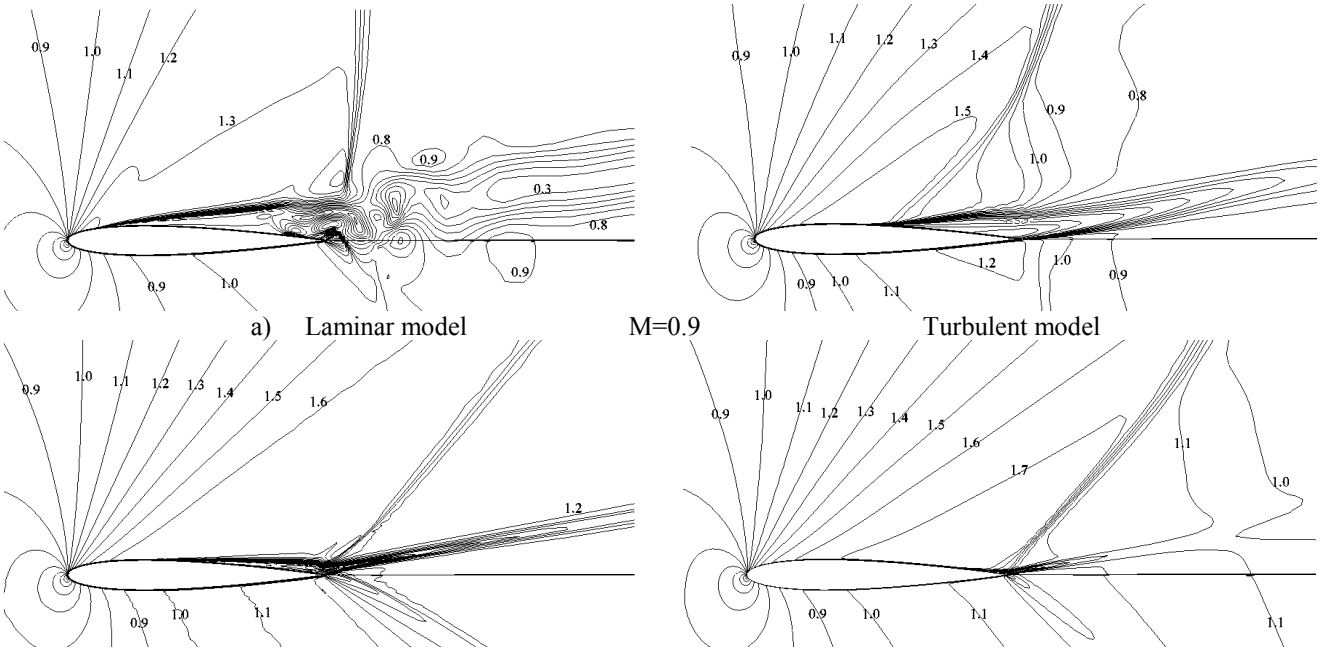

a) Laminar model M=0.9 Turbulent model

b) Laminar model M=1.0 Turbulent model

Fig. 7. Mach Number isolines for M=0.9 a) and M=1.0 b) turbulent and laminar cases for NACA0012 at angle of attack α=10°.

Local Mach number isolines are shown in Fig. 7. These figures illustrate flow fields in the vicinity of NACA-0012 airfoil. Most differences in flow fields for laminar and turbulent models are obtained in subsonic case (M_∞=0.9, Fig. 7a). For laminar model separation of boundary layer occurs near the leading edge, trailing shockwave interacts with shear layer. As a result unsteady flow field occurs, and will be considered bellow. For turbulent model at Mach number M_∞=0.9 (Fig 7a.) the solution is steady. And separation zone dimension is less than that one in laminar case.

For the transonic and supersonic cases flow fields are approximately the same (Fig 7b.).

3.2 Features of unsteady airflow

During investigation great attention were paid to unsteady behaviors of aerodynamics coefficients in laminar case at Mach number M_∞=0.9. Figs. 8-10 represent dependences of coefficients on dimensionless time (t/t^*, $t^*=L/V_\infty$) at angels of attack α=5°, 10°, 15° respectively.

General analysis shows the existence of high frequency and low frequency components.

High frequency harmonic is due to generation, development and separation of vortex from the profile surface. Low frequency component approximately corresponds to time of vortex passing through all numerical area. Additional investigations with more greater numerical region are needed for reasoning of this assumption.

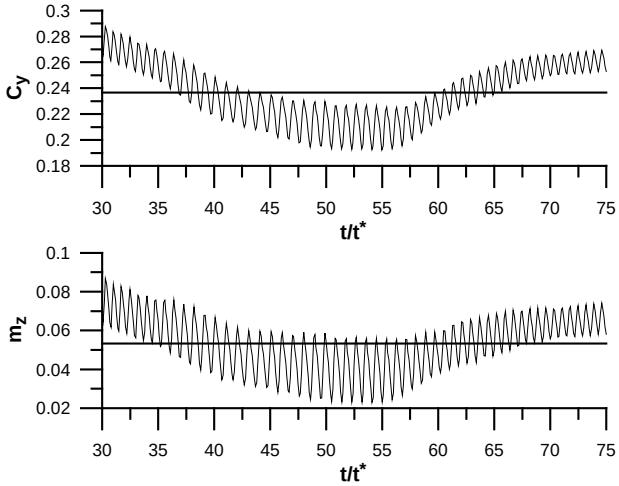

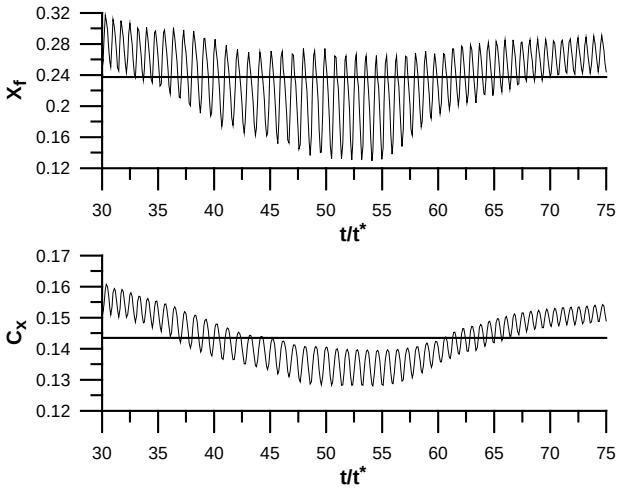

Fig. 8. Dependence of drag, lift, pitching coefficient and aerodynamic center position on dimensionless time for NACA0012 at angle of attack α=5° and Mach number M =0.9

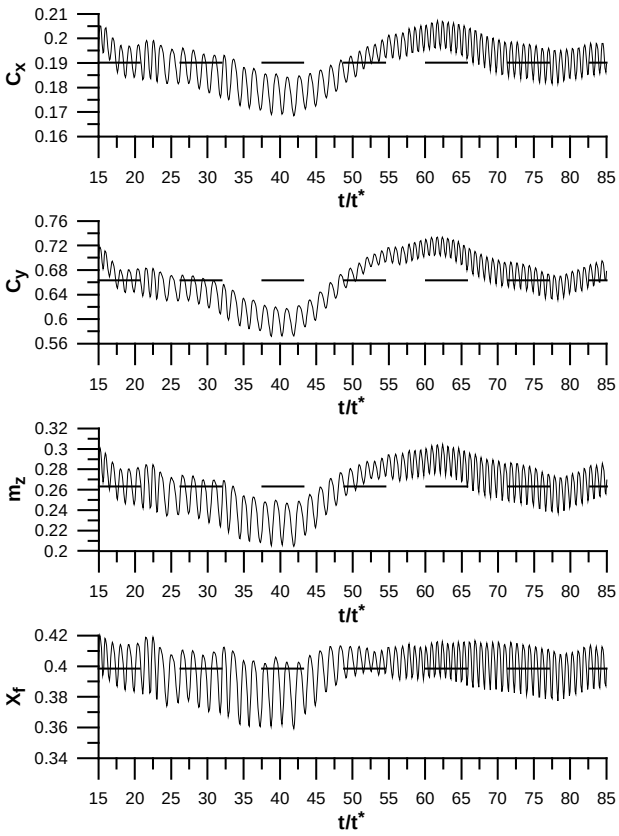

Fig. 9. Dependence of drag, lift, pitching coefficient and aerodynamic center position on dimensionless time for NACA0012 at angle of attack α=10° and Mach number M =0.9

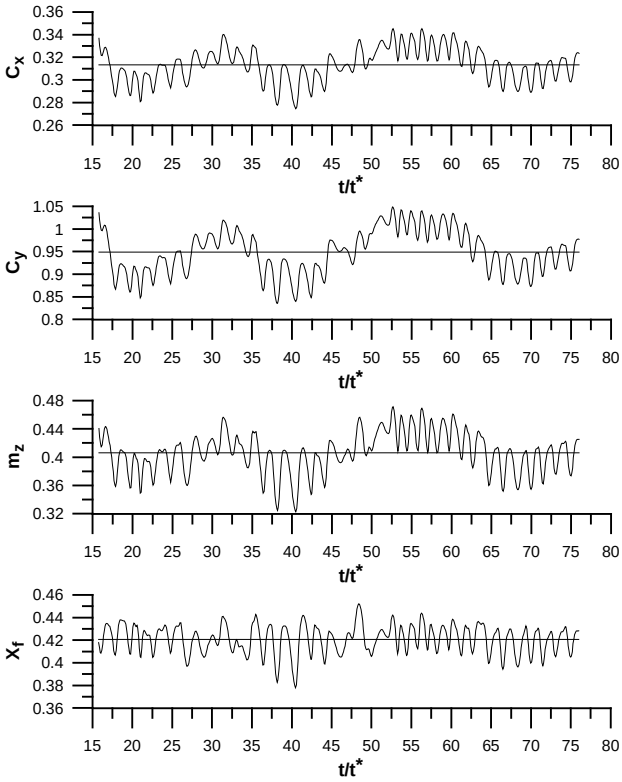

Fig. 10. Dependence of drag, lift, pitching coefficient and aerodynamic center position on dimensionless time for NACA0012 at angle of attack α=15° and Mach number M =0.9

To analyze more accurate the high frequency component the Fourier transformations of coefficients were made. Spectrum of drag, lift, pitching coefficient and aerodynamic center position at different angles of attack are presented in Fig. 11.

The downtrend of fundamental frequency at angle of attack is evident. At α=5° and α=10° additional harmonics appear.

Relative deviations of drag, lift, pitching coefficient and aerodynamic center position vs. angle of attack are shown in Fig.12. Decreasing of relative deviations is due to an increasing of average value. Absolute deviation remains approximately the same with the increasing of angle of attack.

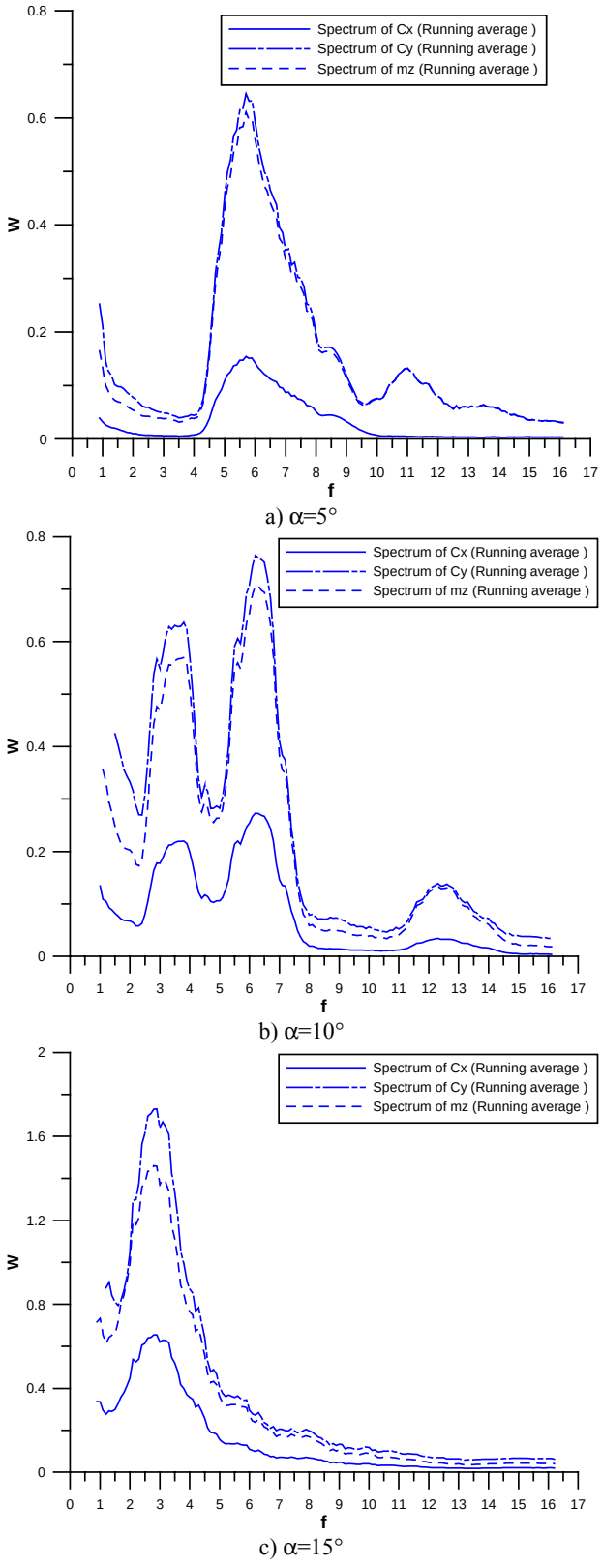

Fig. 11. Spectrum of drag, lift and pitching coefficient for NACA0012 at different angles of attack and Mach number M =0.9

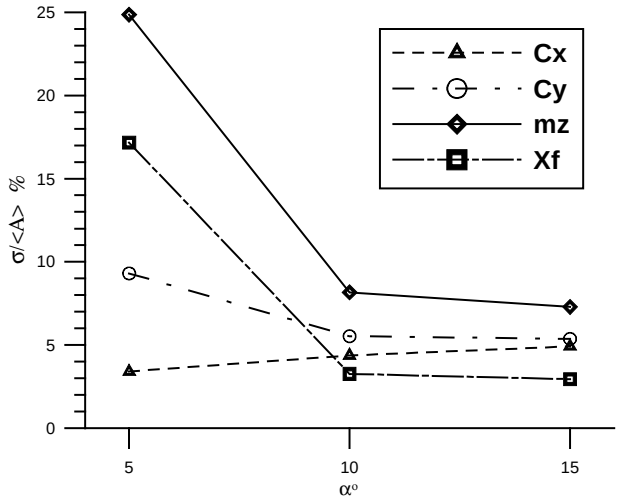

Fig. 12. Relative standard deviation for NACA0012 at deferent angles of attack and Mach number M =0.9

3.3 Double-edge airfoil

Numerical investigations of the flow over double-edge profile at M_∞=0.9 are provided to compare unsteady behavior of aerodynamic characteristics with the data obtained for the profile NACA-0012. The comparison of frequency functions of the flows over two different profiles shows, that the base regularities are the same. The distribution of aerodynamics characteristics of double-edge profile in dependence on time for the angle of attack 10° shows, particularly, an increasing of an amplitude of high frequency vibrations in comparison with the flow over the profile NACA-0012. Nevertheless The frequencies are approximately equal for two cases under consideration studied.

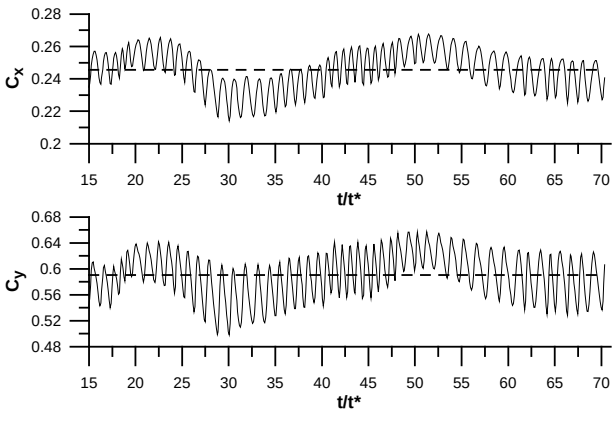

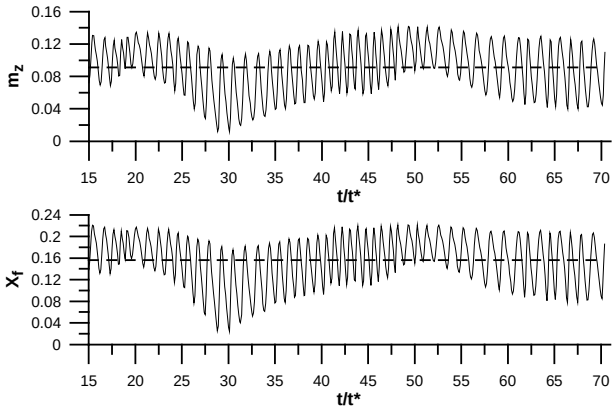

Fig. 13. Dependence of drag, lift, moment coefficient and aerodynamic center position on dimensionless time for double-edge profile at angle of attack α=10° and Mach number M =0.9

3.4 Turbulent results for high angle of attack

Numerical investigations of the flow over the profile NACA-0012 at large angles of attack for turbulent flow model are provided. The dependencies of the base aerodynamic characteristics of the profile for the angles of attack $0°\le\alpha\le30°$ at $Re_\infty=10^6$ are given in the Figs. 14. The behavior of lift force coefficient is evidence of the presence of linear and nonlinear zones and maximum values of C_y.

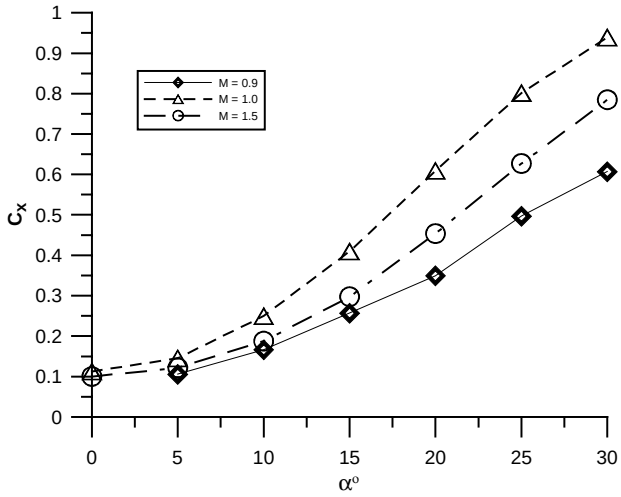

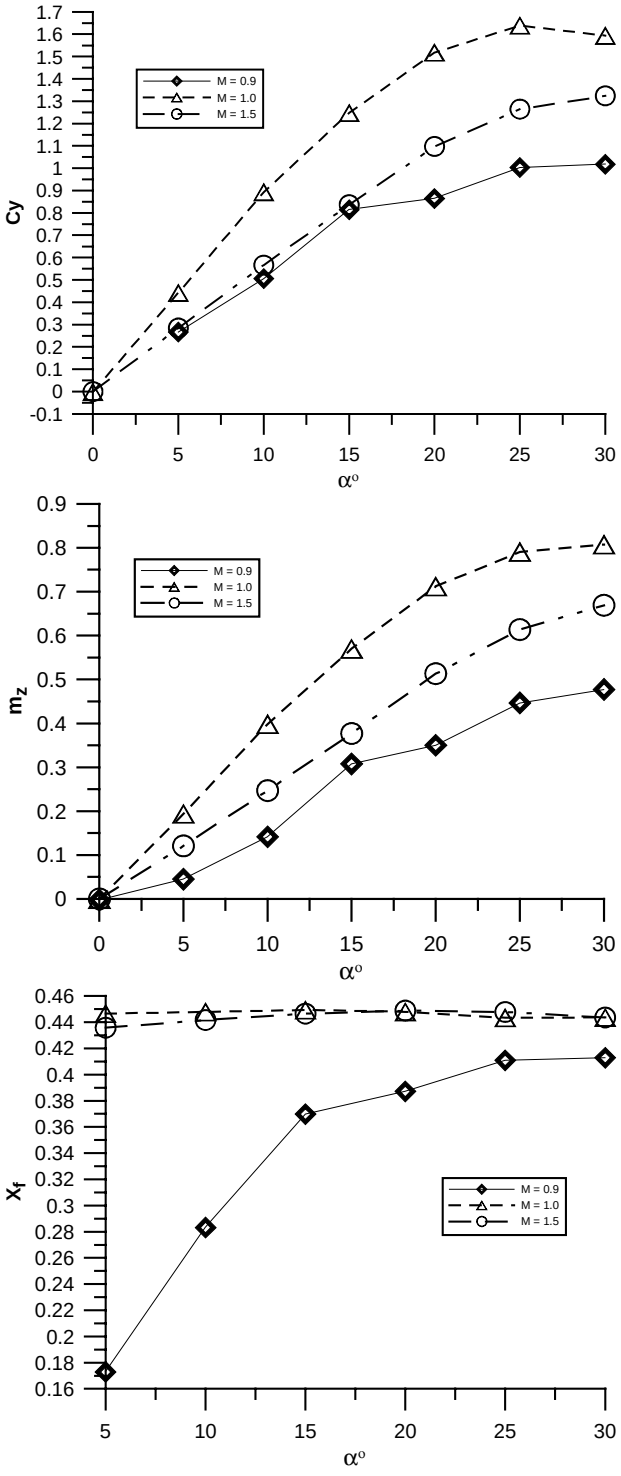

Fig. 14. Dependence of drag, lift, pitching coefficient and aerodynamic center position on angle of attack for NACA0012 with Mach number M =0.9

4 Conclusions

- Program codes for numerical simulation of the Navier-Stokes equations for laminar and turbulent gas models is developed.
- Numerical investigations of the flow over the NACA-0012 profile and double-edge one for transonic flow are provided.
- The steady numerical solutions for all free stream flow parameters are obtained for turbulent flow model. The solution at M_∞=0.9 for laminar flow model is unsteady, the steady solutions are obtained at large Mach numbers.
- The frequency analysis of aerodynamic characteristics of unsteady flow over the profile illustrated the decreasing of the fundamental harmonic with the increasing of angle of attack.
- Numerical flow investigations over the profile NACA-0012 at large angle of attack enabled to determine, particularly, the maximum value of the lift coefficient.

5 Acknowledgment

Author thanks Drs. I. Yegorov and V. Ivanov for help and support in fulfilling of this work.

References

[1] Julian D. Cole, L. Pamela Cook, *Transonic aerodynamics.* Elsevier Science Publisher B.V., 1986.

[2] Christianivich S.A., *Mechanics of Continues Media.* Nauka, Moscow, 1981.

[3] Grozdovsky G.L., Nikolsky A.A., Svishev G.P., Taganov G.I., *Supersonic gas flows in perforated bounds.*, Mashinostroenie, Moscow 1967.

[4] Terry L. Holst, Viscous Transonic Airfoil Workshop Compendium of Results, *AIAA Paper*, 87-1460.

[5] Coakley T. J., and Huang P.G., Turbulence modeling for high speed flows, *AIAA Paper*, 92-0436.

[6] Ivanov D.V., Obabko A.V. and Yegorov I.V., Simulation of separated flows on the base of differential turbulence model, *AIAA Paper*, 97-1861.